



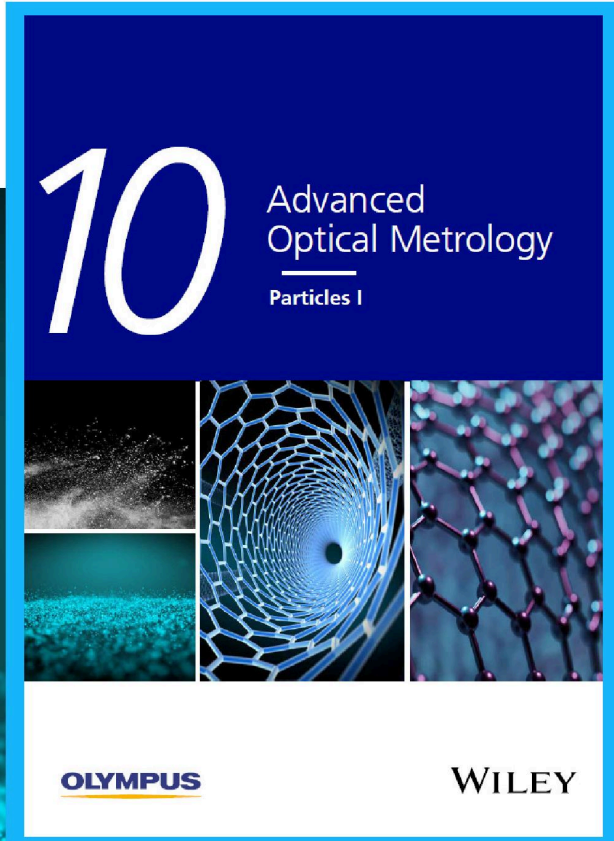
# Particles I

Access the latest eBook →

Particles: Unique Properties,  
Uncountable Applications

Read the latest eBook and  
better your knowledge with  
highlights from the recent  
studies on the design and  
characterization of micro-  
and nanoparticles for  
different application areas.

[Access Now](#)



This eBook is sponsored by

**OLYMPUS**<sup>®</sup>

**WILEY**

# On the Role of Collective Electrostatic Effects in Electronic Level Pinning and Work Function Changes by Molecular Adlayers: The Case of Partially Fluorinated DNTTs Adsorbed Flat-Lying on Various Metals and Hetero-Structures

Maximilian Dreher, David Cornil, Matthias W. Tripp, Ulrich Koert, Jérôme Cornil, and Gregor Witte\*

Modifying the work function of metal electrodes by monolayers of molecules with specifically tailored electronic properties is a versatile tool, but such chemical modifications often also affect the adsorption geometry and packing density, making microscopic modeling difficult. Using scanning tunneling microscopy, it is shown that the recently synthesized partially fluorinated dinaphthothienothiophenes (DNTTs) adopt the same interface structure on different metal substrates independent of the degree of fluorination. Combining Kelvin probe measurements and density functional theory (DFT) calculations, a highest occupied molecular orbital (HOMO) pinning effect for such  $F_x$ DNTTs on Au(111) and Ag(111) induced by collective electrostatic interactions in the monolayer is observed. Since the adsorption of weakly interacting molecules such as the  $F_x$ DNTTs is not restricted to specific surfaces as is the case with SAMs, this concept is extended to metal substrates with quite different work function values. For a low work function surface such as Cs(110), a lowest unoccupied molecular orbital (LUMO) pinning effect is predicted at the theoretical level. Since such alkali metal surfaces are not experimentally accessible, a well-defined Cs monolayer on Cu(100) as a low work function substrate is used instead. For this substrate, however, a variation is observed in the LUMO energies and the work function as a function of the degree of fluorination. This is attributed to the formation of a second interface dipole at the buried Cs/Cu interface, which is modulated with the degree of fluorination and competes with the dipole at the outer molecule/Cs interface. Such a second internal interface dipole, which can be modified by the top layer, has to be considered when going to more complex heterointerfaces.

## 1. Introduction

The intrinsic electronic properties of organic semiconductors (OSCs) can be tailored flexibly by today's chemical synthesis. Transferring this approach also to the frontier electronic energy levels of OSCs adlayers would be a powerful tool for controlling interfacial electronic effects and for adjusting the work function of metallic substrates, and hence reducing the charge carrier injection barriers of organic device architectures.<sup>[1–6]</sup> However, going to the condensed matter, the actual electronic properties of such OSC adlayers exhibit usually drastic changes compared to their isolated states. According to classical electrostatics, the change in the work function through a monolayer depends on the vertical component of the total dipole moment  $\mu_{\perp}$  and the packing density of the molecules. Usually,  $\mu_{\perp}$  can be decomposed into two rather independent components.<sup>[7–10]</sup>

- (i) The interface dipole  $\mu_{\text{int}}$  is associated to charge reorganization processes at the interface, which on one hand is governed by charge transfer between molecule and substrate due to a difference

M. Dreher, G. Witte  
Fachbereich Physik  
Philipps-Universität Marburg  
D-35032 Marburg, Germany  
E-mail: gregor.witte@physik.uni-marburg.de

 The ORCID identification number(s) for the author(s) of this article can be found under <https://doi.org/10.1002/admi.202200361>.

© 2022 The Authors. Advanced Materials Interfaces published by Wiley-VCH GmbH. This is an open access article under the terms of the Creative Commons Attribution-NonCommercial-NoDerivs License, which permits use and distribution in any medium, provided the original work is properly cited, the use is non-commercial and no modifications or adaptations are made.

D. Cornil, J. Cornil  
Laboratory for Chemistry of Novel Materials  
University of Mons (UMONS)  
Mons BE-7000, Belgium  
M. W. Tripp, U. Koert  
Fachbereich Chemie  
Philipps-Universität  
D-35032 Marburg, Germany

DOI: 10.1002/admi.202200361

in their chemical potentials or chemical bonds to the substrate and on the other hand by the push back effect that decreases the surface spill-out and hence the surface dipole of the bare metal substrate by Pauli repulsion.<sup>[11]</sup>

- (ii) The permanent dipole of the molecule  $\mu_{\text{mol}}$  projected onto the surface normal.

Since a chemical functionalization of molecules is often accompanied by changes in their adsorption geometry and/or packing density yielding hardly predictable adsorption areas per molecule, which in turn also affect the work function, it appears quite difficult to independently study the formation of the interface dipole  $\mu_{\text{int}}$ . Interestingly, covalently anchored self-assembled monolayers (SAMs) can be functionalized easily through their molecular backbone via electroactive substituents without perturbing their surface area  $A$ , which was successfully used to modify the work function shift on several substrates.<sup>[12–14]</sup> However, for congeneric SAMs, it was also found recently, that despite quite different HOMO levels of the various molecular entities, the resulting charge transfer at the interface and hence the interface dipole and work function change can be almost the same. Thus, counterintuitively, the new HOMO levels of the adlayer are almost equal due to collective electrostatic effects, which in literature has been referred to by some of us as HOMO level pinning.<sup>[15]</sup>

It is worth stressing that we deliberately avoid using the terminology of Fermi level pinning that has been used extensively to describe the special scenario in which the unperturbed HOMO level of the molecule is above (or the LUMO level below) the Fermi level of the metal. In particular, Fermi level pinning is invoked in the integer charge transfer model typically applied to passivated metal surfaces in contact with OSCs, i.e., in a very weak coupling regime.<sup>[16]</sup> In a simple picture, this model implies that the HOMO level of the organic material cannot lie above the Fermi level  $E_F$  (respectively the LUMO below the Fermi level) of the electrodes, in which case a full charge transfer would occur from the molecule to the metal to reposition the HOMO level below  $E_F$  (or from the metal to the molecule to reposition the LUMO above  $E_F$ ). When the Fermi level lies in the gap of the organic molecule, a Fermi level pinning can also occur in the presence of a significant coupling between the two components and is then driven by the principle of chemical potential equalization (typically associated with  $E_F$  for the metal and corresponding to the midgap value  $(IP + EA)/2$  for the organic semiconductor) both for standing up and flat-lying molecules. Such a Fermi level pinning can be best evidenced by considering a series of closely related molecules. Previously, it was theoretically shown that the HOMO level can be aligned independently of the chemical substitution of the conjugated entity in a single molecule break junction in contrast to the situation prevailing for the isolated compounds;<sup>[17]</sup> in this case, the pinning effect arises from a change in the amplitude of the interface dipole as a function of the HOMO energy in the isolated molecule. Fermi level pinning also rationalizes that the alignment of the HOMO level in SAMs is weakly affected when changing the nature of the metallic electrode due to the modulation of the interface dipoles.<sup>[18]</sup> On the other hand, describing changes in the electronic structure of a single molecule when embedded in a

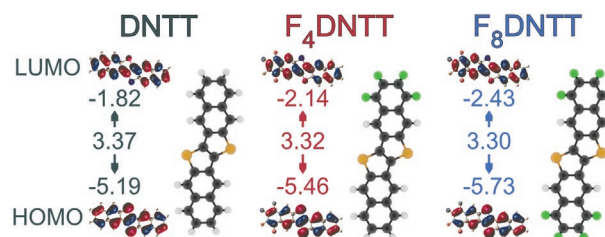


**Figure 1.** HOMO/LUMO energy levels (in eV) of several partially fluorinated DNTTs were calculated via DFT with the B3LYP functional. Corresponding frontier orbitals are depicted next to the energy levels.

solid-state medium due to collective (cooperative) electrostatic effects has received much attention over the years.<sup>[19–21]</sup> However, it is much less recognized and discussed that a HOMO pinning can be observed with respect to the Fermi level for several closely related derivatives due to such effects. In this case, the pinning occurs without any variation in the amplitude of the interfacial charge transfer, thus in stark contrast with the principle of equalization of chemical potentials. This has been observed theoretically in highly ordered systems such as SAMs, without any role played by the Fermi level of the metallic electrode.<sup>[7,15]</sup> This implies that cooperative effects can wipe out the impact of chemical derivatization. This specific HOMO pinning effect has recently been observed experimentally in SAM-based molecular junctions containing a three-ring phenylene ethynylene oligomer and substituted derivatives.<sup>[15]</sup> Although SAMs enable to study of the influence of  $\mu_{\perp}$  on the change in the work function independently of  $A$ , the upright molecular geometry causes a non-negligible tunnel barrier for charge carriers, which limits their use for device applications.<sup>[22]</sup> In addition, the wet chemical processing of SAMs restricts them essentially to noble metal substrates and does not allow to probe low work function surfaces such as alkali metals and to examine whether there is also a possible LUMO pinning effect. An idealized system would therefore be a set of non-covalently bound, flat-lying molecules whose energetic levels can be modified without changing their adsorption geometry.

## 2. Results and Discussion

In this study, we show that the recently synthesized partially fluorinated dinaphthothienothiophenes ( $F_x$ DNTTs,  $x = 0, 4, 8$ ) meet these requirements perfectly and thus enable such an investigation.<sup>[23]</sup> Since the modification of the electronic properties of noble metal surfaces by molecular adlayers has already been discussed in detail in the literature,<sup>[7,16,24–37]</sup> which demonstrates a controlled work function shift by organic mono- and thin multilayer films, we only briefly describe our experimental and theoretical results on the work function changes of the Ag[Au](111) substrates investigated at the beginning in order to validate our methodology. In the next step, we then analyzed the modification of a low work function metal surface with the example of cesium. While Cs crystal surfaces are only theoretically accessible due to their high chemical reactivity and low thermal stability, we have instead used epitaxial Cs monolayers on Cu(100) to mimic a low work function alkali metal surface

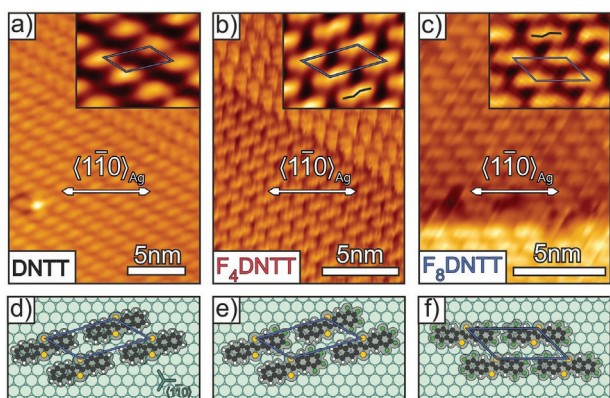


**Figure 2.** a–c) STM images of a nominal monolayer (0.2 nm) of  $F_x$ DNTT on Ag(111). Samples were held at 110 K during measurement to reduce ad molecular diffusion ( $U_{\text{bias}} = -1.92$  V,  $I_t = 60$  pA). d–f) Corresponding structure models.

that enables coverage dependent work function measurements for the various  $F_x$ DNTTs.

As depicted in **Figure 1**, the HOMO and LUMO levels of the  $F_x$ DNTTs shift on a theoretical level toward lower energies with an increasing degree of fluorination, while the optical band gap remains almost constant in full consistency with experimental spectra.<sup>[23]</sup> The interface structure of the non-fluorinated DNTT on the noble metal surfaces Ag(111) and Au(111) was extensively studied previously yielding completely flat-lying molecules with a molecular surface area of  $A = 1.3$  nm<sup>2</sup>.<sup>[38,39]</sup> With this knowledge, we performed scanning tunneling microscopy measurements of all three DNTT derivatives on Ag(111), which are depicted in **Figure 2**.

A comparison of the structure models (cf. **Figure 2d–f**) shows that the  $F_4$ DNTT monolayer adopts the exact same unit cell and consequently the same area per molecule as the non-fluorinated DNTT. Only the unit cell of the  $F_8$ DNTT monolayer is slightly azimuthally rotated compared to the other two derivatives, but exhibits the same molecular area. Since the investigated unit cells on Ag(111) are almost independent of the degree of fluorination and the non-fluorinated DNTT adopts the same unit cell both on Ag(111) and Au(111), we assume that the  $F_x$ DNTTs have similar unit cells also on Au(111). Consequently, this set of  $F_x$ DNTTs monolayers provides an excellent model system in which electronic properties are modulated without changing the flat-lying adsorption geometry. Thereby, any permanent dipole moments along the  $z$ -direction arising from the molecular backbone are safely excluded, which allows to study solely the influence of the HOMO/LUMO positions on the resulting interface dipoles without limitations to specific surfaces.

In the next step, we performed in situ Kelvin probe (KP) measurements of those  $F_x$ DNTTs monolayers on Au(111) as well as on Ag(111) in order to probe the work function change they induce to the metal surfaces. As depicted in **Figure 3a**, all  $F_x$ DNTTs decrease the work function of the bare Au(111) from 5.3 eV down to 4.6 eV upon deposition of a nominal monolayer. A similar trend is observed for Ag(111), which is shifted from 4.5 eV down to 3.9 eV. Complementary, we analyzed the  $F_x$ DNTT monolayers by means of DFT calculations based on

the PBE functional, using the structure models deduced from the STM measurements discussed above (see SI for full details of the modeled structures). Since the primary goal of the theoretical modeling is to rationalize qualitatively the experimental trends, we have first assessed whether we could neglect van der Waals corrections in order to reduce the computational time. The comparison of the two sets of data obtained for  $F_4$ DNTT on Au, Ag, and Cs/Cu points to very similar trends, with actually a quite good quantitative agreement for most of the calculated parameters (see SI). As a result, only DFT/PBE data will be discussed in the remaining of the paper. Doing so, the calculated theoretical work functions of bare gold (5.17 eV) and silver (4.43 eV) are in good quantitative agreement with those gathered experimentally. Moreover, a similar final work function of 4.6 eV is obtained for each modeled  $F_x$ DNTT/Au(111) interface, in full consistency with the experimental data. The same trends are also recovered for  $F_x$ DNTT/Ag(111) interfaces in spite of a small difference between the computed (3.7 eV) and measured (3.9 eV) WFs. This leads us to the conclusion that the WF shift ( $\Delta\Phi$ ) is independent of the degree of fluorination of the DNTT also on a theoretical level.

This is in contradiction to the simple picture, where the chemical potential  $\mu_{\text{chem}}$  of the isolated molecules changes with the degree of fluorination and hence the amount of charge transfer, resulting in a different work function shift. Actually, the HOMO states of the three derivatives in the monolayer are pinned to the same value by collective effects (cf. **Figure 3b**); this is in contrast to the isolated molecules, which reveal an energetic spread of this orbital of 0.54 eV (as indicated by the colored arrows in **Figure 3b**). From an experimental point of view, a similar decrease of the WF in the order of 0.5–0.7 eV could also indicate a pure pushback effect without any charge transfer. We have already shown in a previous study that the non-fluorinated DNTT causes an additional WF shift when going to multilayer films ( $\Delta\Phi_{\text{DNTT,Ag}} = -0.9$  eV and  $\Delta\Phi_{\text{DNTT,Au}} = -1.0$  eV),<sup>[39]</sup> which is either caused by some charge transfer or by a permanent dipole moment of the film. Since the DNTT molecule has no significant dipole moment, there has to be a charge transfer between the molecular layer and the metal substrates. It is quite interesting that this HOMO pinning effect, which is schematically shown in **Figure 3c** on the right side, is not only present for covalently bound SAMs with molecular backbones in close contact but also for weakly interacting systems like the  $F_x$ DNTT molecules lying flat on noble metal surfaces. Here, as described before, collective electrostatic effects lead to HOMO levels in the adsorbed organic layer, which are pinned to a specific value, such that the work function shift is similar for all  $F_x$ DNTTs. This situation differs from a Fermi level pinning, in which the equalization of the electronic levels originates from a charge transfer of different amplitude between the organic layer and the metal, leading in turn to different vacuum shifts and hence work function shifts among the  $F_x$ DNTTs, as depicted schematically in **Figure 3c** on the left-hand side.

These results motivated us to further investigate whether there is also a corresponding LUMO pinning effect within the same molecular systems for surfaces with a very low work function, which has not been conducted experimentally in literature yet. Due to the quite weak interaction of these organic

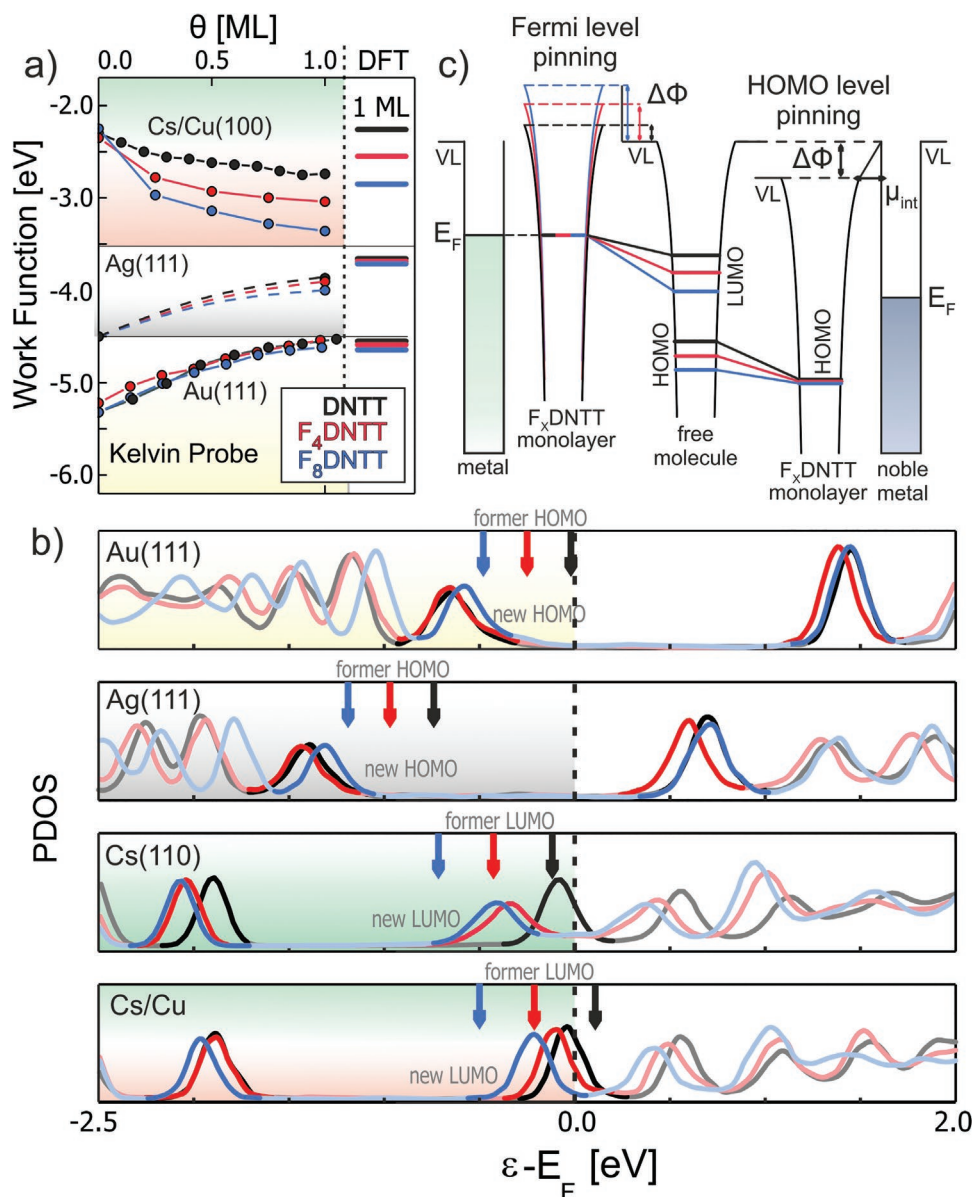


**Figure 3.** a) Coverage dependent KP measurements for  $F_x$ DNTTs on Au/Ag(111) and on Cs/Cu(100). On the right side corresponding DFT predictions of the WF for 1 ML of  $F_x$ DNTT. b) Calculated projected density of states (PDOS) of nominal  $F_x$ DNTT monolayers with respect to the Fermi levels of the corresponding substrates. Colored arrows mark the involved energetic levels of the isolated molecules. c) Energy level scheme that compares Fermi level pinning (in this case at the LUMO levels) and the HOMO level pinning effect.

molecules with the substrate, the deposition is not limited to specific metals as it is the case for SAMs, which allows us to further investigate their electronic properties on alkali metals. However, their low thermal stability and high reactivity make corresponding experiments on alkali metal single crystals impossible and have therefore hardly been considered in the literature so far. Only the usage of alkali metals as dopants for organic thin films has been shown, which leads to a certain Fermi level pinning effect in the molecular adlayers.<sup>[40]</sup> Therefore, we first investigated the effect of  $F_x$ DNTT layers on the work function of alkali metal surfaces on a theoretical level for the case of cesium. To compare the results with the previously studied densely packed fcc(111) surfaces of Au and

Ag, we considered the corresponding bcc(110) surface of Cs. At our DFT level, our calculation yields a work function for a Cs(110) slab of 1.73 eV, which is in close agreement with the work function reported for polycrystalline Cs films of 1.82 eV.<sup>[41]</sup> To simulate the  $F_x$ DNTT adlayer, starting from the previously determined monolayer structure, we approximated it by a commensurate superstructure on the Cs(110) surface (see SI). The DFT geometry optimization revealed only a slight bending of the adsorbates but no evidence for strong chemical interaction with the substrate. For the  $F_x$ DNTT monolayers, the calculated work functions are significantly increased and yield almost the same values for each molecular species,  $\Phi_{\text{DNTT}}$ : 2.9 eV,  $\Phi_{\text{F4DNTT}}/\Phi_{\text{F8DNTT}}$ : 2.8 eV

(see Table S5 in the SI), which in fact confirms the presence of a LUMO pinning effect (as depicted schematically in Figure 3c on the left).

In order to make such a substrate with low work function also experimentally accessible, we followed an approach introduced before by Papageorgopoulos et al. using a highly ordered monolayer of Cs adsorbed on Cu(100).<sup>[42]</sup> Such an adlayer reveals a complete wetting of the copper surface and forms an epitaxial monolayer with a quasi-hexagonal structure. In addition, the monolayer is chemically and thermally more stable due to the strong coupling to the metal support,<sup>[42–45]</sup> thus providing a densely packed metal surface with a low work function of 2.3 eV, which is only slightly larger than for Cs bulk. As shown in Figure 3a, the WF increases with coverage upon deposition of  $F_x$ DNTT molecules and the monolayer value shifts stronger with higher degree of fluorination:  $\Phi_{\text{DNTT}} = 2.7$  eV,  $\Phi_{\text{F}_4\text{DNTT}} = 3.0$  eV,  $\Phi_{\text{F}_8\text{DNTT}} = 3.3$  eV. Hence, these results do not evidence a LUMO pinning predicted from the DFT calculations on the Cs(110) slab.

In order to decipher this apparent discrepancy, we also examined the adsorption of the  $F_x$ DNTTs molecular films on Cs/Cu(100) in the frame of DFT. In order to make this complex system calculable, we first approximated the point-on-line epitaxy of the Cs adlayer<sup>[45]</sup> by a commensurate monolayer and also considered the molecular film as commensurate (for details see SI). While the calculation reproduces well the trend that the higher fluorinated species cause a large WF increase (cf. Figure 3a), the absolute values are slightly smaller, which can be explained by the somewhat lower packing density used in the DFT structures. The calculations reveal a negligible molecular distortion thus indicating only weak interaction, which is experimentally confirmed by reproducing the WF of the bare Cs monolayer after thermal desorption of the  $F_x$ DNTT adlayers at about 470 K without any indication of dissociation. Therefore, the influence of bending of adsorbed  $F_x$ DNTT molecules, which can lead to a relevant contribution of a perpendicular molecular dipole and thus to a work function change,<sup>[46]</sup> is unlikely to explain the present observation. On the other hand, the corresponding PDOS depicted in Figure 3b exhibits small but notable differences in the LUMO levels of the molecular adlayer between

the  $F_x$ DNTTs, especially a similar energetic order as the isolated molecular states, thus indicating indeed the absence of a LUMO pinning effect.

To understand in more detail why the work function changes and especially why the trend for the various  $F_x$ DNTTs is so different for the Cs(110) and Cs/Cu(100) substrates, we have analyzed the adsorption induced charge density profile at the  $F_x$ DNTT/metal interface obtained at the DFT level. Figure 4 compares the differential charge density distribution  $\Delta\rho(z)$  of the  $F_x$ DNTT monolayers adsorbed on the various surfaces (averaged over the adlayer unit cell) with respect to the bare substrates along the surface normal ( $z$ -axis). The adsorption of all  $F_x$ DNTTs on the Ag(111) and Au(111) surfaces results in a similar charge redistribution within the admolecules and the interface regardless of the degree of fluorination. Adsorption of all  $F_x$ DNTT monolayers leads to an increase of the total charge of about  $Q_{\text{FxDNTT}} = +0.3|e|$  on silver and  $+0.4|e|$  on gold, which reflects a charge transfer from the molecules into the noble metal (cf. Table S3, SI). A closer look at Figure 4b,c shows that the center of the transferred charges is located mostly at the top of the metal layer, thus pointing to the co-existence of a push-back effect through the molecular adlayer and (weak) chemisorption. Since the corresponding adsorption-induced molecular dipoles have similar spatial expansions and the same area density, the metal work functions of both noble metals are decreased by almost the same amount. In contrast to the noble metals, the calculations for the Cs(110) slab show a distinct charge transfer from the substrate into the molecules ( $Q_{\text{DNTT}}: -1.15|e|$ ,  $Q_{\text{F}_4\text{DNTT}}: -1.45|e|$ ,  $Q_{\text{F}_8\text{DNTT}}: -1.56|e|$ ), leading to an oppositely oriented interface dipole and thus an increased work function (cf. Table S4, SI). Moreover, the center of positive transferred charges in the first cesium layer are located in the center of the atoms in contrast to the Ag/Au surfaces, hence reflecting a stronger charge transfer into the Cs layer. A closer look at the charge profile in the metal (Figure 4d) reveals that in addition to the first layer of cesium, the second layer is also charged, but negatively. Thus, the large electron depletion (i.e., positive charge accumulation) at the first cesium layer caused by the charge transfer into the molecules induces a charge reorganization of the Cs bulk and leads to a smaller negative charge accumulation in the second Cs layer below. Consequently, this

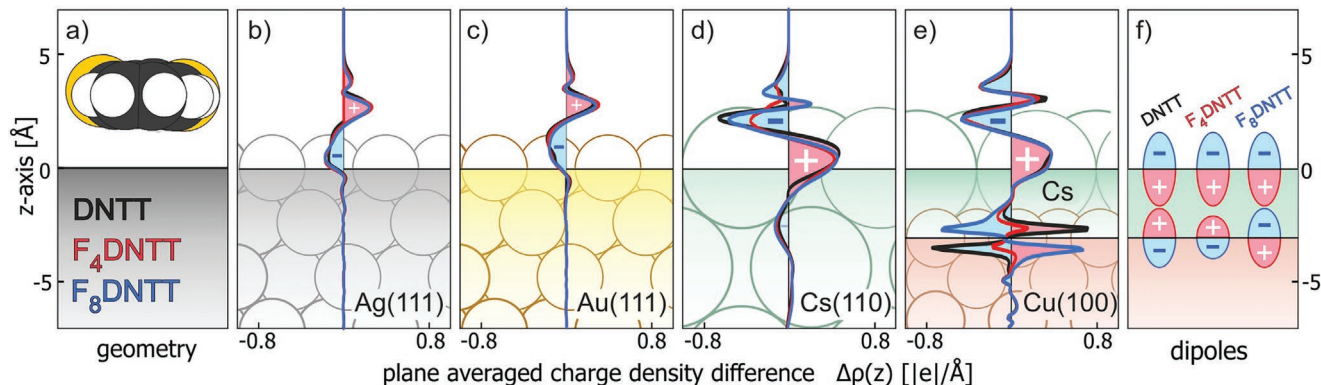


**Figure 4.** a) Vertical adsorption geometry of  $F_x$ DNTT monolayers. b–e) Adsorption induced planar averaged charge density differences along the  $z$ -direction for a nominal monolayer of  $F_x$ DNTT on the various substrates. f) Schematic representation of the formed interface dipoles between  $F_x$ DNTT/Cs and Cs/Cu.

causes the formation of an additional internal dipole between the first and second Cs layer. This internal dipole and the dominating dipole at the molecule/Cs interface sum up and yield an overall similar work function change for the various adlayers, although there are small differences in the charge transfer between the fluorinated and non-fluorinated DNTT derivatives. Thus, interestingly a LUMO pinning effect is present (at least) for the monolayer of fluorinated  $F_x$ DNTTs on Cs(110) at a theoretical level.

Despite a similar work function as for the Cs(110) surface, the experimentally realized Cs/Cu(100) heterostructure shows a clearly different interface electronics and distinctly different work function changes for the various  $F_x$ DNTT adlayers. The corresponding theoretical analysis reveals a yet larger charge transfer from the Cs layer into the molecular adlayer, which increases with the degree of fluorination ( $Q_{\text{DNTT}}$ :  $-1.36|e|$ ,  $Q_{\text{F4DNTT}}$ :  $-1.51|e|$ ,  $Q_{\text{F8DNTT}}$ :  $-1.59|e|$ ). While this causes the Cs layer to be positively charged, as in the case of the Cs(110) substrate, the polarization at the Cs/Cu(100) interface is quite different. As depicted in Figure 4e (a magnified version is provided in Figure S8, Supporting Information), an additional dipole moment is formed at the internal Cs/Cu interface, whose magnitude and direction depend on the degree of fluorination of the  $F_x$ DNTT admolecules. While the adsorption-induced charge distribution at the outer  $F_x$ DNTT/Cs interface hardly depends on the degree of fluorination of the admolecules, one finds much larger and very different charge distributions at the inner Cs/Cu interface. While a Cs bulk counteracts the charge transfer into the molecules through a charge reorganization within the first 2–3 layers, which leads to similar interface dipoles, this does not occur for the Cs/Cu heterostructure because the metals involved have different chemical potentials. The dipole moment at this internal Cs/Cu interface, which is schematically shown in Figure 4f, adds to the dipole at the metal/molecule interface and significantly contributes to the overall surface dipole and hence to the work functions change. This shows, that although a single layer of cesium can successfully reduce the work function, the internal metal/metal interface significantly contributes to and even dominates the surface energetics. A similar internal charge accumulation effect was also reported for metal/graphene/metal sandwich structures,<sup>[47]</sup> and thus appears to be a general phenomenon occurring for encapsulated 2D-layers supported by metals. This demonstrates that the overall surface electronic properties of such layered systems result from a competitive interaction between the outer and buried interface dipoles.

### 3. Conclusion

To conclude, we were able to demonstrate a HOMO pinning effect, which was first observed for covalently bound SAMs on gold surfaces, also for weakly interacting adsorbates such as the  $F_x$ DNTT monolayers on Au(111) and Ag(111) investigated here. Due to the uniform interface structure of the  $F_x$ DNTTs and their non-confinement to specific substrate surfaces, we were further able to probe the extent of LUMO pinning effect within the same molecular system on low work function metal

surfaces. To do so, we simulated monolayers of the  $F_x$ DNTTs on a Cs(110) slab, which is as densely packed as the (111) faces of gold and silver. Here, we found regardless of a different charge transfer depending on the actual fluorination of the molecules a pronounced LUMO pinning, resulting in an overall similar work function change for the adlayer. Since single-crystalline alkali metal surfaces cannot be prepared, we used cesium monolayers stabilized on Cu(100), which also provide an atomic-flat hexagonal surface with a low work function of about 2.3 eV. In contrast to the expected LUMO pinning, we observed both experimentally and theoretically a different work function change upon adsorption of the various  $F_x$ DNTT molecules, which is dependent on the degree of fluorination. A detailed analysis of the actual charge profiles of that molecular adlayer/metallic monolayer/metal substrate hetero-interface reveals an additional charge accumulation and formation of a dipole moment at the internal interface between the Cs layer and the metal substrate that contributes to the overall interface dipole. The latter finding appears to be characteristic for molecular adlayers adsorbed on metallic heterolayers as well as sandwich structures of 2D materials and different metals where dipoles are formed at the outer and the buried interfaces. To investigate these phenomena, it was necessary to systematically study a prototypical set of congeneric organic molecules such as the  $F_x$ DNTTs on several metal substrates with quite different work function values.

### 4. Experimental Section

**Sample Preparation:** The single crystalline Ag(111) and Au(111) samples were prepared by epitaxial growth of the specific metal onto freshly cleaved and degassed mica substrates under high-vacuum conditions (typical thickness: 100 nm). This yielded highly ordered (111) surfaces with atomically flat terraces extending more than 100 nm, separated by monoatomic steps.<sup>[48]</sup> Before organic film deposition, the metal surfaces were cleaned in situ by several cycles of  $\text{Ar}^+$  sputtering at low energy ( $E_{\text{ion}} \approx 500$  eV), in order to avoid incorporation of Ar atoms in the metal surface, and annealing ( $\approx 750$  K) until a sharp LEED pattern with low background signal was observed and no contaminations were found via STM. For the Cu(100) single crystal slightly higher annealing temperatures of about 800 K were applied. On top of the clean Cu(100) surface, we deposited cesium films from SAES getters dispenser with typical heating currents of 6.0 A, which were monitored by a quartz crystal microbalance (QCM). As described by Papageorgopoulos et al.<sup>[42,43]</sup> cesium exhibits a stabilized, hexagonal-shaped monolayer on top Cu(100), while subsequent grown layers will desorb quickly at room temperature after deposition. DNTT (Sigma–Aldrich, purity: 99%) and new synthesized  $F_4$ DNTT/ $F_8$ DNTT thin films were prepared by organic molecular beam deposition from aluminum crucibles of a resistively heated Knudsen cell under high-vacuum conditions, monitored also by a QCM.

**Sample Characterization:** The interface structures of the molecular thin films were characterized under ultra-high vacuum (UHV) conditions by means of STM (OMICRON VT STM XA), operated in constant current mode (typically  $I_t = 400$  pA) and using etched tungsten tips. The work functions of all samples were measured in the same UHV chamber by means von KP technique (Besocke Delta Phi GmbH, Kelvin Probe S). Highly ordered pyrolytic graphite (HOPG, NT-MDT, quality: A) samples were used to reference the gathered contact potentials with a value of 4.4 eV.<sup>[49]</sup>

**DFT Calculations:** For the electronic properties of the various ( $F_x$ ) DNTT/metal interfaces, calculations have been carried out at a periodical DFT level, as implemented in the 4.1 version of the SIESTA code.<sup>[50,51]</sup> We used a MeshCutoff of 250 Ry with the exchange-correlation treated

using the PBE functional. Core electrons were described using Troullier-Martins pseudopotentials while a DZP (double- $\zeta$  + polarization) numerical atomic basis set was used for the treatment of the valence electrons with the following configurations: H 1s<sup>1</sup>, C 2s<sup>2</sup>2p<sup>2</sup>, F 2s<sup>2</sup>2p<sup>6</sup>, S 3s<sup>2</sup>3p<sup>4</sup>, Au 6s<sup>1</sup>5d<sup>10</sup>, Ag 5s<sup>1</sup>4d<sup>10</sup>, Cu 4s<sup>1</sup>3d<sup>10</sup>, Cs 6s<sup>1</sup>5p<sup>6</sup>. In our experience, this theoretical approach yields very similar electronic properties when compared to a planewave-based method such as VASP.<sup>[52]</sup>

## Supporting Information

Supporting Information is available from the Wiley Online Library or from the author.

## Acknowledgements

The authors acknowledge support by the German Science Foundation (Deutsche Forschungsgemeinschaft, DFG) project-ID 223848855-SFB 1083 “structure and dynamics of internal interfaces”. The computational resources was provided by the Consortium des “Equipements de Calcul Intensif” (CÉCI) funded by the Belgian National Fund for Scientific Research (F.R.S.-FNRS) under Grant 2.5020.11. J.C. was an FNRS Research Director.

Open access funding enabled and organized by Projekt DEAL.

## Conflict of Interest

The authors declare no conflict of interest.

## Data Availability Statement

The data that support the findings of this study are available from the corresponding author upon reasonable request.

## Keywords

alkali metal surfaces, density functional theory, heterostructures, interface dipole, organic/metal interfaces, work function

Received: February 17, 2022

Revised: March 21, 2022

Published online:

- [1] I. H. Campbell, J. D. Kress, R. L. Martin, D. L. Smith, N. N. Barashkov, J. P. Ferraris, *Appl. Phys. Lett.* **1997**, *71*, 3528.
- [2] E. L. Hanson, J. Guo, N. Koch, J. Schwartz, S. L. Bernasek, *J. Am. Chem. Soc.* **2005**, *127*, 10058.
- [3] K. Asadi, F. Gholamrezaie, E. C. P. Smits, P. W. M. Blom, B. d. Boer, *J. Mater. Chem.* **2007**, *17*, 1947.
- [4] N. Koch, *ChemPhysChem* **2007**, *8*, 1438.
- [5] P. Stoliar, R. Kshirsagar, M. Massi, P. Annibale, C. Albonetti, D. M. de Leeuw, F. Biscarini, *J. Am. Chem. Soc.* **2007**, *129*, 6477.
- [6] J. Kim, Y. S. Rim, Y. Liu, A. C. Serino, J. C. Thomas, H. Chen, Y. Yang, P. S. Weiss, *Nano Lett.* **2014**, *14*, 2946.
- [7] G. Heimel, L. Romaner, J.-L. Brédas, E. Zojer, *Phys. Rev. Lett.* **2006**, *96*, 196806.
- [8] P. C. Rusu, G. Giovannetti, G. Brocks, *J. Phys. Chem. C* **2007**, *111*, 14448.
- [9] L. Romaner, G. Heimel, C. Ambrosch-Draxl, E. Zojer, *Adv. Funct. Mater.* **2008**, *18*, 3999.
- [10] M. L. Sushko, A. L. Shluger, *Adv. Mater.* **2009**, *21*, 1111.
- [11] G. Witte, S. Lukas, P. S. Bagus, C. Wöll, *Appl. Phys. Lett.* **2005**, *87*, 263502.
- [12] G. Heimel, L. Romaner, E. Zojer, J.-L. Bredas, *Acc. Chem. Res.* **2008**, *41*, 721.
- [13] G. Heimel, F. Rissner, E. Zojer, *Adv. Mater.* **2010**, *22*, 2494.
- [14] C. Schmidt, A. Witt, G. Witte, *J. Phys. Chem. A* **2011**, *115*, 7234.
- [15] S. Rodriguez-Gonzalez, Z. Xie, O. Galangau, P. Selvanathan, L. Norel, C. van Dyck, K. Costuas, C. D. Frisbie, S. Rigaut, J. Cornil, *J. Phys. Chem. Lett.* **2018**, *9*, 2394.
- [16] S. Braun, W. R. Salaneck, M. Fahlman, *Adv. Mater.* **2009**, *21*, 1450.
- [17] C. van Dyck, V. Geskin, A. J. Kronemeijer, D. M. de Leeuw, J. Cornil, *Phys. Chem. Chem. Phys.* **2013**, *15*, 4392.
- [18] B. Kim, S. H. Choi, X.-Y. Zhu, C. D. Frisbie, *J. Am. Chem. Soc.* **2011**, *133*, 19864.
- [19] C. Poelking, M. Tietze, C. Elschner, S. Olthof, D. Hertel, B. Baumeier, F. Würthner, K. Meerholz, K. Leo, D. Andrienko, *Nat. Mater.* **2015**, *14*, 434.
- [20] G. D'Avino, L. Muccioli, F. Castet, C. Poelking, D. Andrienko, Z. G. Soos, J. Cornil, D. Beljonne, *J. Phys. Condens. Matter* **2016**, *28*, 433002.
- [21] N. Ferri, A. Ambrosetti, A. Tkatchenko, *Phys. Rev. Mater.* **2017**, *1*, 26003.
- [22] F.-R. F. Fan, J. Yang, L. Cai, D. W. Price, S. M. Dirk, D. V. Kosynkin, Y. Yao, A. M. Rawlett, J. M. Tour, A. J. Bard, *J. Am. Chem. Soc.* **2002**, *124*, 5550.
- [23] M. W. Tripp, D. Bischof, M. Dreher, G. Witte, U. Koert, *Eur. J. Org. Chem.* **2021**, *8*, 1295.
- [24] H. Ishii, K. Sugiyama, E. Ito, K. Seki, *Adv. Mater.* **1999**, *11*, 605.
- [25] N. Koch, S. Duhm, J. P. Rabe, A. Vollmer, R. L. Johnson, *Phys. Rev. Lett.* **2005**, *95*, 237601.
- [26] N. Koch, S. Duhm, J. P. Rabe, S. Rentenberger, R. L. Johnson, J. Klankermayer, F. Schreiber, *Appl. Phys. Lett.* **2005**, *87*, 101905.
- [27] H. Yamane, D. Yoshimura, E. Kawabe, R. Sumii, K. Kanai, Y. Ouchi, N. Ueno, K. Seki, *Phys. Rev. B* **2007**, *76*, 979.
- [28] N. Gonzalez-Lakunza, I. Fernández-Torrente, K. J. Franke, N. Lorente, A. Arnau, J. I. Pascual, *Phys. Rev. Lett.* **2008**, *100*, 156805.
- [29] S. Duhm, A. Gerlach, I. Salzmänn, B. Bröker, R. L. Johnson, F. Schreiber, N. Koch, *Org. Electron.* **2008**, *9*, 111.
- [30] N. Koch, A. Gerlach, S. Duhm, H. Glowatzki, G. Heimel, A. Vollmer, Y. Sakamoto, T. Suzuki, J. Zegehnagen, J. P. Rabe, F. Schreiber, *J. Am. Chem. Soc.* **2008**, *130*, 7300.
- [31] S. A. DiBenedetto, A. Facchetti, M. A. Ratner, T. J. Marks, *Adv. Mater.* **2009**, *21*, 1407.
- [32] G. Heimel, S. Duhm, I. Salzmänn, A. Gerlach, A. Strozecka, J. Niederhausen, C. Bürker, T. Hosokai, I. Fernandez-Torrente, G. Schulze, S. Winkler, A. Wilke, R. Schlesinger, J. Frisch, B. Bröker, A. Vollmer, B. Detlefs, J. Pflaum, S. Kera, K. J. Franke, N. Ueno, J. I. Pascual, F. Schreiber, N. Koch, *Nat. Chem.* **2013**, *5*, 187.
- [33] M. Oehzelt, N. Koch, G. Heimel, *Nat. Commun.* **2014**, *5*, 4174.
- [34] J.-P. Yang, F. Bussolotti, S. Kera, N. Ueno, *J. Phys. D: Appl. Phys.* **2017**, *50*, 423002.
- [35] F. Widdascheck, A. A. Hauke, G. Witte, *Adv. Funct. Mater.* **2019**, *29*, 1808385.
- [36] E. Zojer, T. C. Taucher, O. T. Hofmann, *Adv. Mater. Interfaces* **2019**, *6*, 1900581.
- [37] J. J. Cartus, A. Jeindl, O. T. Hofmann, *ACS Omega* **2021**, *6*, 32270.
- [38] Y. Hasegawa, Y. Yamada, T. Hosokai, K. R. Koswattage, M. Yano, Y. Wakayama, M. Sasaki, *J. Phys. Chem. C* **2016**, *120*, 21536.
- [39] M. Dreher, D. Bischof, F. Widdascheck, A. Huttner, T. Breuer, G. Witte, *Adv. Mater. Interfaces* **2018**, *5*, 1800920.
- [40] L. Yan, N. J. Watkins, S. Zorba, Y. Gao, C. W. Tang, *Appl. Phys. Lett.* **2001**, *79*, 4148.
- [41] T. J. Lee, B. H. Blott, B. J. Hopkins, *Appl. Phys. Lett.* **1967**, *11*, 361.
- [42] C. A. Papageorgopoulos, *Solid State Commun.* **1978**, *27*, 1069.
- [43] C. A. Papageorgopoulos, *Phys. Rev. B* **1982**, *25*, 3740.
- [44] P. Fouquet, G. Witte, *Phys. Rev. Lett.* **1999**, *83*, 360.

- [45] P. Fouquet, G. Witte, *Surf. Sci.* **2000**, 454–456, 256.
- [46] O. T. Hofmann, D. A. Egger, E. Zojer, *Nano Lett.* **2010**, 10, 4369.
- [47] C. Gong, D. Hinojos, W. Wang, N. Nijem, B. Shan, R. M. Wallace, K. Cho, Y. J. Chabal, *ACS Nano* **2012**, 6, 5381.
- [48] M. Dreher, G. Witte, *Phys. Chem. Chem. Phys.* **2021**, 23, 8023.
- [49] W. N. Hansen, G. J. Hansen, *Surf. Sci.* **2001**, 481, 172.
- [50] J. M. Soler, E. Artacho, J. D. Gale, A. García, J. Junquera, P. Ordejón, D. Sánchez-Portal, *J. Phys.: Condens. Matter* **2002**, 14, 2745.
- [51] A. García, N. Papior, A. Akhtar, E. Artacho, V. Blum, E. Bosoni, P. Brandimarte, M. Brandbyge, J. I. Cerdá, F. Corsetti, R. Cuadrado, V. Dikan, J. Ferrer, J. Gale, P. García-Fernández, V. M. García-Suárez, S. García, G. Huhs, S. Illera, R. Korytár, P. Koval, I. Lebedeva, L. Lin, P. López-Tarifa, S. G. Mayo, S. Mohr, P. Ordejón, A. Postnikov, Y. Pouillon, M. Pruneda, et al., *J. Chem. Phys.* **2020**, 152, 204108.
- [52] D. Cornil, H. Li, C. Wood, G. Pourtois, J.-L. Brédas, J. Cornil, *ChemPhysChem* **2013**, 14, 2939.